6th European Conference on Computational Mechanics (ECCM 6)
7th European Conference on Computational Fluid Dynamics (ECFD 7)
1115 June 2018, Glasgow, UK

PERFORMANCE ANALYSIS OF A PLUNGING WING AT LOW REYNOLDS NUMBER

Charles E. Badoe[*,†], **Zheng-Tong Xie**[*] **and Neil D. Sandham**[*]

[*] Aerodynamics and Flight Mechanics Group, Faculty of Engineering and the Environment, University of Southampton, Southampton, SO17 1BJ, United Kingdom.
[†] Corresponding author: ceb1r14@soton.ac.uk

Key words: Dynamic stall, Large-eddy simulations

Abstract. Simulations of the flow over a heaving NACA0012 wing are conducted to study the effects of the separated flow phenomena for a pre-stall and post-stall wing condition. An extensively validated high fidelity large-eddy simulation (LES) approach is used to examine the unsteady aerodynamic loads and flow structures at Reynolds number Re_c = 20,000. We consider the effect of varying reduced frequencies from k=0.47-0.94 for a normalized amplitude of A/c=0.5 and angles of attack of 5° and 15°, representing the pre-stall and post-stall conditions respectively. Comparison to experiment show good agreement for lift and moments as well as flow structures. Characteristic phenomena of dynamic stall are analysed with emphasis on the leading edge vortex LEV development. Transition to turbulence is observed alongside the LEV and the disturbances reach the wing surface.

1 INTRODUCTION

The unsteady aerodynamics of oscillating wings has received much attention in recent years. A wide range of studies, including those of [1-3] has increased our knowledge of the unsteady flow patterns and transient effects, including flow instabilities and vortex shedding, primarily from a two-dimensional perspective. These studies have been motivated by the flight characteristic of natural flyers. Oscillating wings experience a dynamic stall behaviour, which exhibits large hysteresis on the lift and moment when the time varying angle of incidence goes beyond its static stall angle, due to the unsteady wing motion [4]. It has been found [5] that the leading edge vortex (LEV) plays a critical role in the lift enhancement. In static wing aerodynamics, near the stall angle the flow is highly unsteady and separated. Measurements [6] have shown that the unsteady flow has a low coherency in the spanwise direction, even for a two-dimensional geometry. However an unsteady heaving wing motion can increase coherency resulting in organised vortical structures that greatly influence the unsteady loads.

There have been numerous investigations into the dynamic stall behaviour of oscillating wings using unsteady Reynolds-averaged Navier-Stokes (RANS) methods [7-9]. Most of this research has shown that RANS methods are not sufficient to predict such a time

dependent flow structure. For example, when the frequency of a periodically oscillating wing is increased, it induces large shed vortices and downstream vorticity [10]. Wang et al.[9] showed that RANS methodologies are not suitable in predicting such flow details and suggested that advanced approaches such as direct numerical simulation (DNS) or large eddy simulation (LES) should be used to capture the details of such flows.

The majority of the DNS and LES computational studies on the aerodynamic behaviour of oscillating wings, and especially in heaving motions, tend to focus on either near-wake structures, or spanwise vortical structures at high reduced frequency ($k \geqslant 2.0$) and low amplitude ($A/c \leqslant 0.1$), with much less attention paid to much lower reduced frequency and higher amplitude [10], due to the large computational resources involved to capture the flow details. In an effort to capture more completely the flow behaviour in these specific conditions at a much reduced computational cost, [11] used LES to simulate the unsteady flow over a pitching airfoil. Investigations were made for k = 0.25-1.0 and Re_c = 135,000. Pitching was achieved by using a dynamic mesh that deformed the cells each time step, allowing the wing boundary to move within the domain. The effect of the aerodynamic forces on the pitching airfoil was the focus of their work. The approach was able to predict the trends in the coefficients of lift, drag and moments compared with the experimental data. Spanwise vorticity components and instantaneous streamlines also compared well with experiments.

In the current contribution, we use a similar approach to [11] to examine the physics behind the dynamic stall of a heaving wing. The paper focuses on two key points: (i) assessing the performance of the LES approach for the prediction of the aerodynamic loads through detailed comparison with experimental water tunnel data, and (ii) detailed analysis of flow instabilities at the leading edge during a heaving cycle.

2 NUMERICAL SIMULATIONS

The LES have been carried carried out using OpenFOAM version 2.3.0. A second order implicit scheme was used for the temporal discretization and the bounded second order (Gamma) scheme[1] [12] was used for the convection term. The time step $\triangle t U_\infty/c$ = 8.0 $\times$ 10^{-4} corresponds to 4000 time steps per cycle. The pimpleDyMFoam solver in OpenFOAM was used which is a transient solver for incompressible flow on a moving mesh utilising the PIMPLE (merged PISO-SIMPLE) agorithm. The PIMPLE algorithm includes both under relaxation and velocity correction and is mainly used for transient flows, but without the same courant number constraints of the PISO algorithm. The number of outer iterations was set to two and the number of pressure corrections was set to three. Both the mixed time-scale (MTS) model of [13] and the wall adapting local eddy-viscosity (WALE) model of [14] have been used. The advantages of both models are that the eddy viscosity goes naturally to zero in the wall region, so neither constant adjustments nor damping functions are needed to compute wall bounded flows. Both models have also been credible when applied to transitional flow past wings [9,11] which is one of the key points of the present application.

[1]Gamma = 0.25.

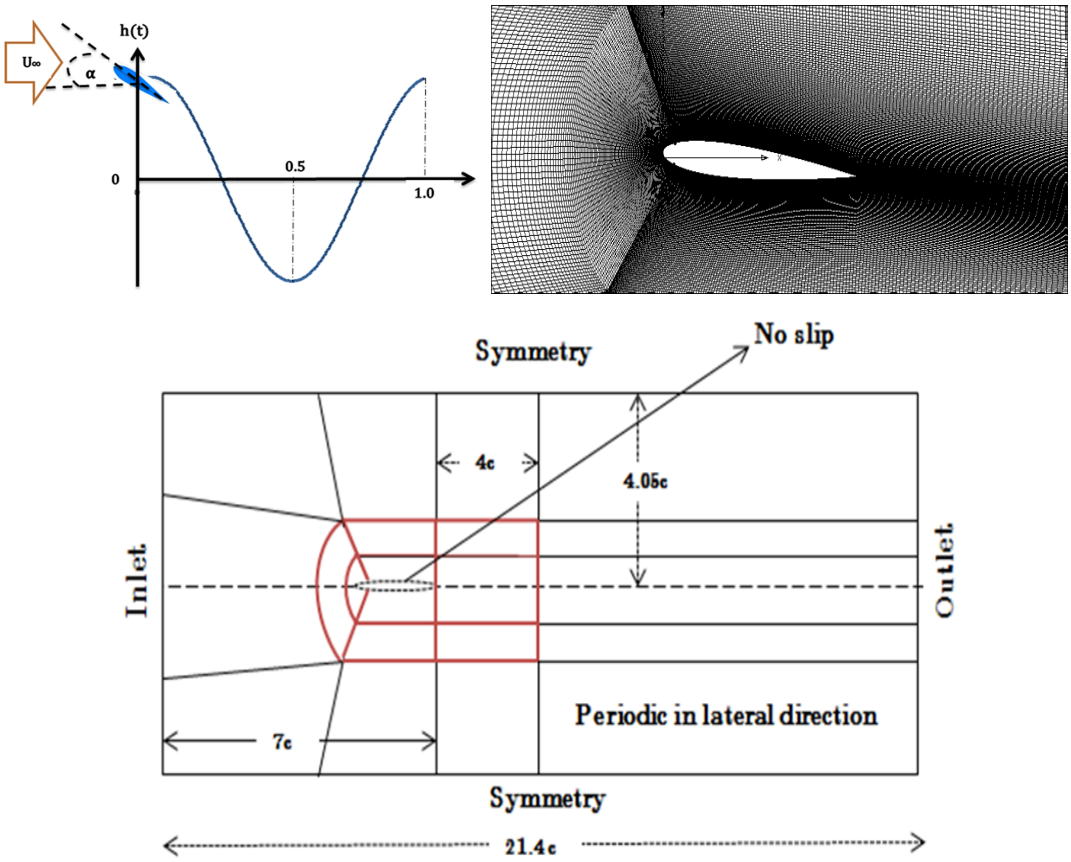

Figure 1: Top-left: heaving motion; Top-right: mesh topology; Bottom: sketch of the domain including applied boundary conditions.

2.1 Simulation parameters and grid generation

The wing section considered in the present study has a NACA-0012 profile with chord $c = 0.0627$m and was modified to include a sharp trailing edge. The wing section has been the subject of a recent experimental investigation [15]. Unsteady and phase averaged computations were conducted with sinusoidal plunging motion $y = A\sin(2\pi ft)$, reduced frequencies $k = 0.47$ and 0.94 and peak to peak amplitude $A/c = 0.5$. A sketch of the computational domain created using Pointwise version 16 is shown in Figure 1. The set-up matches experimental water tunnel conditions in the axial and lateral directions. A C-type grid was adopted close to the wing surface. Away from the wing surface, an H-type grid was used. Grid points were concentrated around the wing boundary layer to capture the transition process. The domain was extruded in the spanwise direction by 0.25c and had a uniform spacing of about 30 to 60 cells, aiming to provide $5 \leq \triangle z^+ \leq 10$ over the wing surface. This span was selected based on a spanwise sensitivity studies, as described in section 3. For the wall normal spacing, the mesh was designed to satisfy a $y^+ \leq 1$ criterion. An approximate $\triangle x^+ \leq 10$ was also achieved on the wing surface. In the near wake region (from the wing trailing edge to a distance of 4 chords) the spacing was kept

uniform and an aspect ratio of 1 was maintained in this region to capture the anticipated near wake vortices. To avoid building separate grids for each angle of attack and also to maintain the strict LES requirements, the blocks surrounding the wing section (denoted in red in Figure 1), together with the wing, were rotated about the quarter chord to the desired neutral angle of attack, with the vertices of those blocks adjusted accordingly to generate low skewed cells and to maintain a good quality mesh in the boundary layer and wake region. Boundary conditions include no-slip and symmetry conditions at the wall and the two lateral boundaries respectively. Periodic conditions were also imposed in the spanwise direction. Heaving computations were started from a previously simulated static condition (static cases were computed for about 10 chord flow pasts) and then run for about 7 cycles. Data was processed from the third cycle onwards.

3 SENSITIVITY STUDIES

3.1 Grid resolution effects

Three different grids were used to provide insight into the impact of grid spacing on the overall prediction of the aerodynamic loads. The grids, labelled G1,G2 and G3 were generated based on the same geometry definition by a systematic $\sqrt{2}$ refinement of the reference structured block-grid. The number of points in all three directions of longitudinal, lateral and span-wise was varied. The grid system used for the analysis is shown in Table 1. Illustration of the grids generated on the wing is also shown in Figure 1 (Top-right) for grid G2. The effect of the grid resolution on the lift and drag coefficient is shown in Figure 2. Data in Figure 2 was taken after the third cycle because we found out that the hysteresis from the successive cycles in general matched well with that of the third cycle. From the grid resolution study it was found that grid resolution had little effect during the wing's downward displacement (i.e. the increasing lift side of the hysteresis loop in Figure 2). There were, however, some quantitative differences during the wing's upwards displacement. This is because of the unsteadiness in flow structure within these regions, where the prominent elements in the flow are the separated shear layer emanating from the leading edge and the development of the trailing edge vortex (TEV). It is crucial that the mesh is fine enough to capture these unsteady flow structures. The results on the coarse grid G1 deviate from the medium grid G2 and fine grid G3, probably due to the fact that the spanwise spacing of $\Delta z/c$=30 is not enough to resolve the details. Although G2 and G3 agree well with each other, there are still some minor differences, which are of the order of the cycle to cycle variations.

3.2 Effect of Subgrid model

Two different subgrid models were used to investigate the effect of the subgrid model on the computed aerodynamic loads, namely the MTS model with model constants C_{MTS} = 0.03 and $C_T = 10$ and the WALE model with model constant $C_w = 0.325$. Grid G2 was used for this study. Good agreement was obtained between the different subgrid models, as seen in Figure 3. The difference between the maximum lift coefficients was less than 0.4% of the two models (C_{Lmax}= 2.74 for MTS and C_{Lmax}=2.73 for WALE model). There

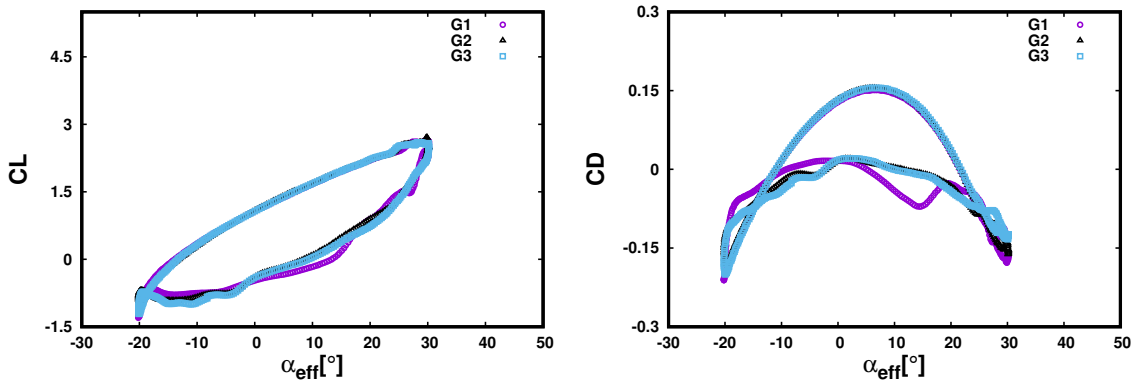

Figure 2: The effect of grid resolution on the computed aerodynamic loads: Lift (left), Drag (right), $\alpha = 5°$, $k = 0.94$ and $A/c = 0.5$.

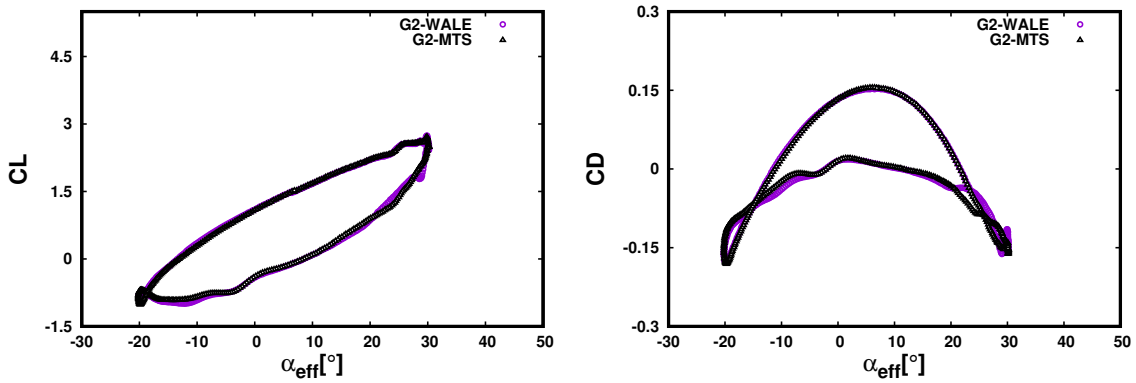

Figure 3: The effect of subgrid model on the computed aerodynamic loads: Lift (left), Drag (right), $\alpha = 5°$, $k = 0.94$ and $A/c = 0.5$.

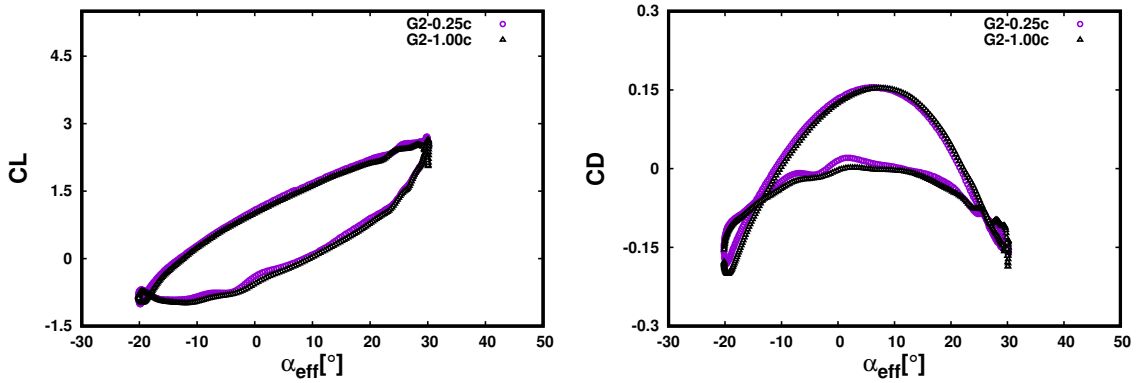

Figure 4: The effect of spanwise domain size on the computed aerodynamic loads: Lift (left), Drag (right), $\alpha = 5°$, $k = 0.94$ and $A/c = 0.5$.

Table 1: Grid and domain parameters, $\alpha = 5°$, $k = 0.94$ and $A/c = 0.5$

$Mesh$	$Size$	N_{AU}	N_{AL}	$\Delta z/c$	$U[c]$	$W[c]$	$H[c]$	$Z[c]$
G1	456×176×30	176	176	0.0083	7.0	14.4	4.05	0.25
G2	645×249×43	249	249	0.0058	7.0	14.4	4.05	0.25
G3	912×352×60	352	352	0.0041	7.0	14.4	4.05	0.25

* NB:Computational domain size normalised by the wing chord length c and grid parameters for heaving wing. U: upstream length; H: domain height; W: wake length; Z: span length; N_{AU}: number of grid points on the wing upper surface; N_{AL}: number of grid points on the wing lower surface; $\Delta z/c$: spanwise spacing

were some minor differences in the lift prediction during the wing's upwards displacement at $\alpha_{eff} = 30°$, where the WALE model produced a localised peak in the lift curve that was not seen for the MTS model.

3.3 Spanwise domain size

In the current computations the spanwise domain size was fixed to 0.25c, similar to values adopted by [16] at comparable Reynolds numbers. In order to verify whether this size was sufficient, additional computations were conducted with a different spanwise size, i.e. s = 0.25c & 1.0c. The corresponding grid was constructed using G2 mesh, and the spacing in the spanwise direction, $\Delta z/c$ was kept fixed. Hence, the grid sizes were 645×249×43 and 645×249×172, representing s=0.25c and s=1.0c respectively. The effect of span width on the computed aerodynamic load is shown in Figure 4. The difference between the maximum lift coefficient was about 1.8% of the two domain widths and occured at $\alpha_{eff} = 30°$. We have also looked into the flow fields (not shown here) and found that the key features of the flow remain unaltered. Similar tendencies has also been found by [16] who carried out investigations on the deep dynamic stall of a plunging wing at comparable Reynolds number to determine the relative importance of the spanwise width on the overall flow structure. According to [16], the limited effect of the span extent on the flow structure is due to the forcing. This behaviour contrasts with unforced flows on bluff bodies where larger spans are usually required. Further extending the span width beyond s=1.0c is not expected to show any significant changes in the aerodynamic loads.

The results of all the different cases are in good agreement with each other, for example, the maximum lift in all cases occurred at $\alpha_{eff} = 30°$ with less than 1.0% difference. For the main set of simulations grid G2, with span s=0.25c and the MTS subgrid model, representing a reasonable compromise in accuracy and computational cost, was chosen.

4 Results

4.1 Mean flow features

A comparison between LES and experimental water tunnel results for the pre-stall and post-stall heaving case is shown in Figure 5, illustrating the variations of the phase averaged lift coefficient as a function of the effective angle of attack as well as the time-averaged

lift as a function of the heaving reduced frequency. The phased-averaged experimental data were obtained through averaging over 55 cycles. As it was not feasible in the present computation to average over such a large number of cycles, the computed phase-averaged data for all comparison purposes have been averaged over three cycles. The LES results shown in Figure 5 agree closely with experiment over the whole heaving cycle in particular at lower reduced frequency (k=0.47). As the reduced frequency increases to k=0.94 there is a slight deviation between LES and the water tunnel measurements especially during the increasing-lift part of the cycle. Specifically, the maximum lift is under-predicted by 10% for the pre-stall angle of attack of $\alpha = 5°$, which is associated with the first LEV formation and its convection. This is also reflected in the time-averaged lift results in Figure 5 (bottom). Note that the sensitivity studies conducted in Figures 2-4 did not show any significant differences in the hysteresis loop, hence the discrepancies cannot be attributed to the mesh, subgrid model or span width. Results from other successive cycles did not also show any big differences. Extending the computations to include averaging over 55 cycles as in the experiment is not expected to provide significant improvement in the mean lift values. Potential causes for the discrepancies include support interference and inflow disturbance effects in the water tunnel experiment, none of which were included in the computations. End-wall effects also play a defining role in oscillating wing aerodynamic load predictions as has been addressed by [16], who showed that the presence of a side wall can induce significant spanwise variations in the leading and trailing edge vortices during the dynamic stall process, thus influencing the aerodynamic loads. In the experiments, the wing had end plates, at the tip and root, however, there was a gap of 2mm between the tip and the end plate, which accounts for about 3% of the chord. As the vortices become more three-dimensional, the gap could influence the tip flow, hence the tip vortex and the aerodynamic load prediction.

A view of the mean flow features is provided in Figures 6 for the pre-stall condition, showing the phase-averaged spanwise vorticity at three phases in the heaving cycle. At t/T=0, the wing is at it maximum displacement. An attached flow is observed and is more defined in the computations compared to the experiment. On the pressure side of the wing, some localised vortices can be seen at about 0.3c. The LES also capture the trailing edge separation and the near-wake vortical structures that were shed from the previous cycle.

As the wing continues to move downwards from t/T=0 to t/T=0.25, it experience an increase in effective angle of attack. Lift and moments change rapidly and the wing starts to undergo the so-called "dynamic stall", which is characterised by the formation of the LEV. The computed and experimental flow structures are in close agreement. A reversed flow can be observed underneath the LEV. The trails of shed vortices from the previous cycle seen in the wake are also in qualitative agreement with the experiment.

As the wing continues to decelerate at t/T=0.5, it reaches its minimum point during the heaving motion. The main LEV has been shed downstream at about 0.5c and the trailing edge vortex (TEV) starts to emerge. The separation region with reversed flow between the main vortex and the secondary one at the leading edge is more prominent compared to t/T=0.25.

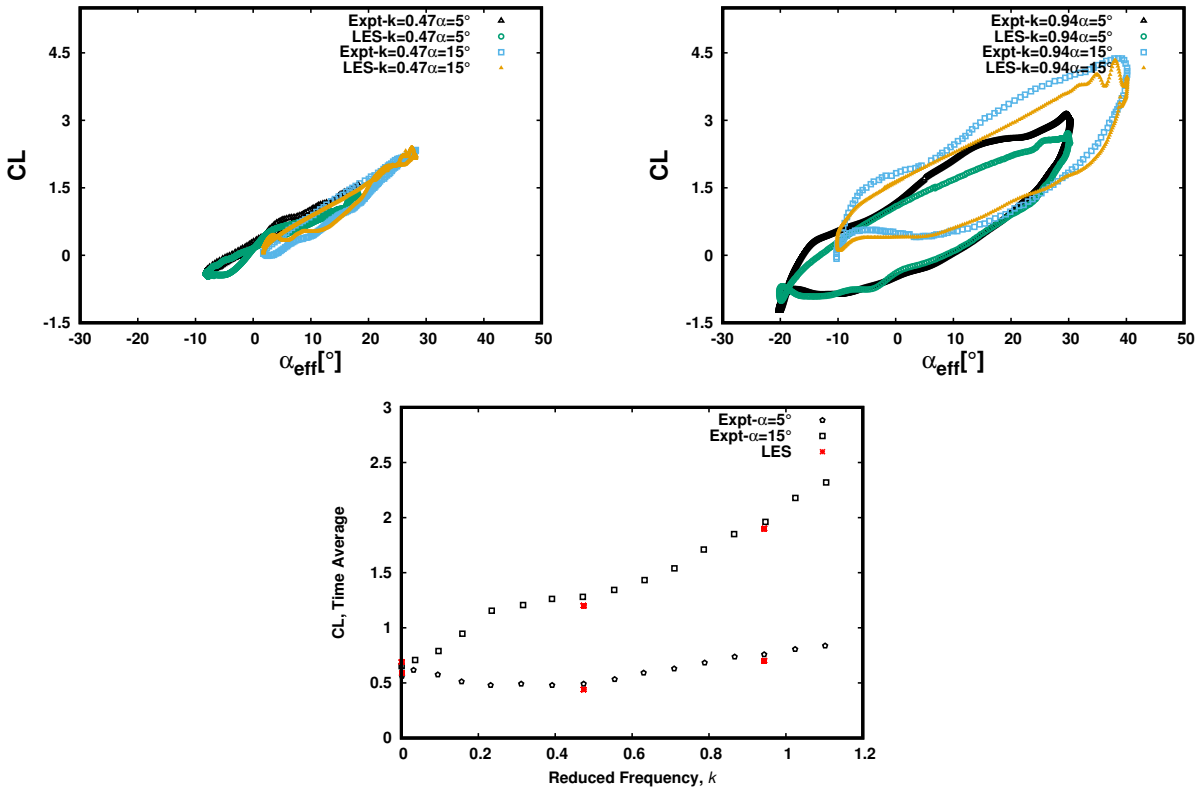

Figure 5: Phase-averaged lift coefficient as a function of the heave-induced effective angle of attack: (Top-Left) $k = 0.47$; (Top-Right) $k = 0.94$; (Bottom) Time-averaged lift as a function of the heaving reduced frequency k, $A/c = 0.5$; $\alpha = 5°$ and $15°$.

4.2 Instantaneous flow features

As the effective angle of attack increases, the LEV is initiated. As the LEV is generated and convects downstream, an increase in lift occurs as the LEV enlarges the effective camber of the wing. The process of transition of the LEV is a significant feature of the dynamic stall process, as it influences the aerodynamic loads. The characteristics of the LEV system and its transition to turbulence are therefore investigated for $\alpha = 5°$, $k = 0.94$ (Figures 7-8). Figure 7(left) shows signals taken using 100 probes placed one cell above the suction surface of the wing evenly distributed at the same chordwise and spanwise location. The signals corresponds to the fluctuating vertical velocity, v' and were staggered by their chordwise (x/c) position relative to the leading edge. The v' signals were taken for one cycle of the heaving motion. High fluctuations are distinguished as regions of high vorticity and may be characterised by flow separation and re-attachment. A closer inspection of Figure 8 shows turbulent structures from the leading edge (at x/c=0.1) up to the mid-chord (at x/c=0.5) between ϕ =65° − 180° (hereafter termed region A). The flow then undergoes transitions and re-laminarises as it approaches the trailing edge (from x/c = 0.5-1.0). The turbulent structures in region A occur during the wing's downwards displacement until the wing reaches its minimum point. Figure 8(c-

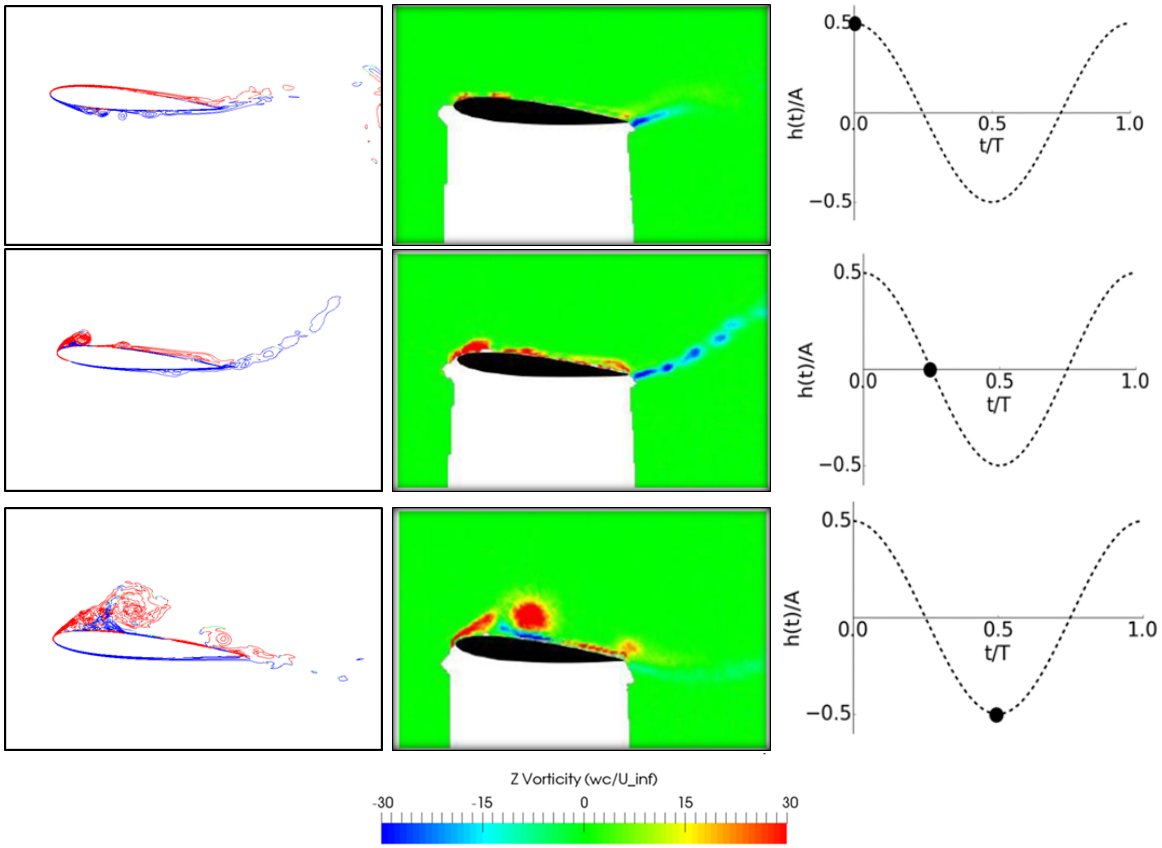

Figure 6: Phased-averaged contour plot of spanwise vorticity for $\alpha = 5^0$, $k = 0.94$ and $A/c = 0.5$: LES(left); Expt(middle)[15]; Displacement (right).

l) shows ten snapshots (in region A) of isosurfaces of instantaneous vorticity magnitude showing three-dimensional flow structures on the suction side of the heaving wing. Figures 8a and b have also been included to emphasise that the boundary layer of the wing was laminar up until ϕ=65°, when the emergence of the first LEV (L1) was observed. L1 is two dimensional in nature with no spanwise variations. The flow is mostly attached with some separation at the trailing edge, as seen in the skin friction plot in Figure 7(right). L1 then grows in size from ϕ=65° − 86°, still retaining its coherent structure. At ϕ=86° three vortices can be observed, namely L1 (now at x/c=0.1), a secondary vortex (L2) upstream of L1 at x/c=0.05, and a third vortex structure (L3) at x/c=0.3. Spanwise instabilities at the leading edge start to appear at ϕ=93°, which is seen more clearly in the surface plot in Figure 8m. The corresponding skin friction plot in Figure 7 (ϕ=93°) shows evidence of separation at the leading edge. L1 starts to breakdown from ϕ=101° − 108°. By ϕ=144°, spanwise instability is more visible. Skin friction plots shows the unsteady boundary layer separates at around x/c=0.2. A single vortex structure characterised by small scale turbulent structures define the flow features in this region. The shedding of L1 continues from ϕ=158°, reaching about 5 chords at ϕ=180° which is also the minimum point during the heaving motion.

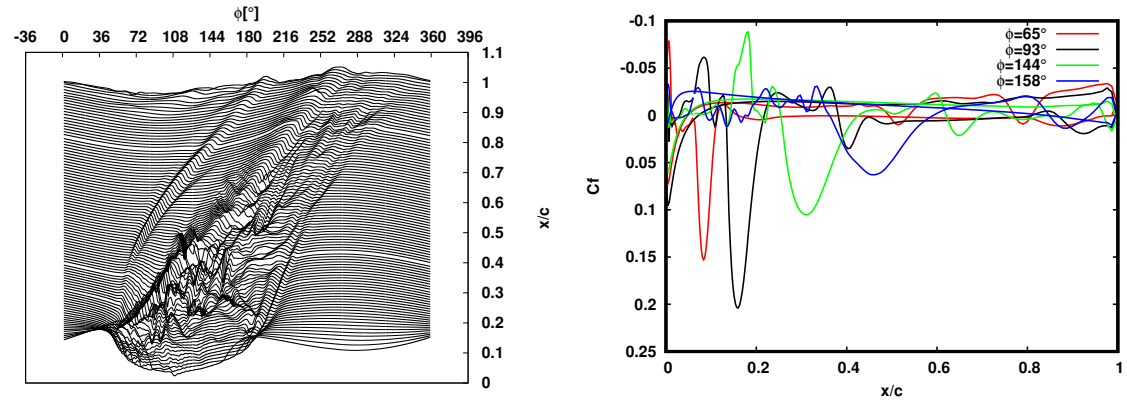

Figure 7: Left:Instantaneous vertical velocity signals v'; Right: skin friction coefficients at $\phi = 65° - 158°$, $\alpha = 5°$, $k = 0.94$ and $A/c = 0.5$.

5 CONCLUSIONS

An advanced LES approach to gain valuable insight into the characteristic phenomena of the dynamic stall process, and more especially the LEV formation and transition, has been presented. Computational results for both aerodynamic loads and mean flow features compared well with experimental water tunnel measurements. Analysis of the mean flow features show that when the angle of attack increases from pre-stall to post-stall, the size of the LEV increases and there is a delay in the laminar to turbulent transition process. The LEV system was found to be two-dimensional in nature with no spanwise variation. However, it exhibits sudden breakdown (at $\phi = 101°$) due to a three-dimensional instability at the span. Transition to turbulence is observed in the LEV and the disturbance are observed down to the wing surface. The transition to turbulence and the LEV shedding process are similar to to those reported in literature [16] at comparable Reynolds number.

Acknowledgements

This work was supported by Engineering and Physical Sciences Research Council (EPSRC) grant EP/M022692/1. The authors acknowledge the use of IRIDIS High Perfomance Computing Facility at the University of Southampton and the UK National Supercomputing Service Archer supported by the EPSRC under grant EP/L000261/1.

REFERENCES

[1] Wang, Z.J. Two dimensional mechanism for insect hovering. *J. Phys Rev.* (2000) **85**:2216–2219.

[2] Lewin, G.C. and Haj-Hariri, H. Modelling thrust generation of a two-dimensional heaving wing in a viscous flow. *J. Fluid Mech.* (2003) **492**:339–362.

[3] Jones, L.E., Sandberg, R.D. and Sandham, N.D. Direct numerical simulation of forced and unforced separation bubbles on a wing at incidence. *J. Fluid Mech.* (2008) **602**:175–207.

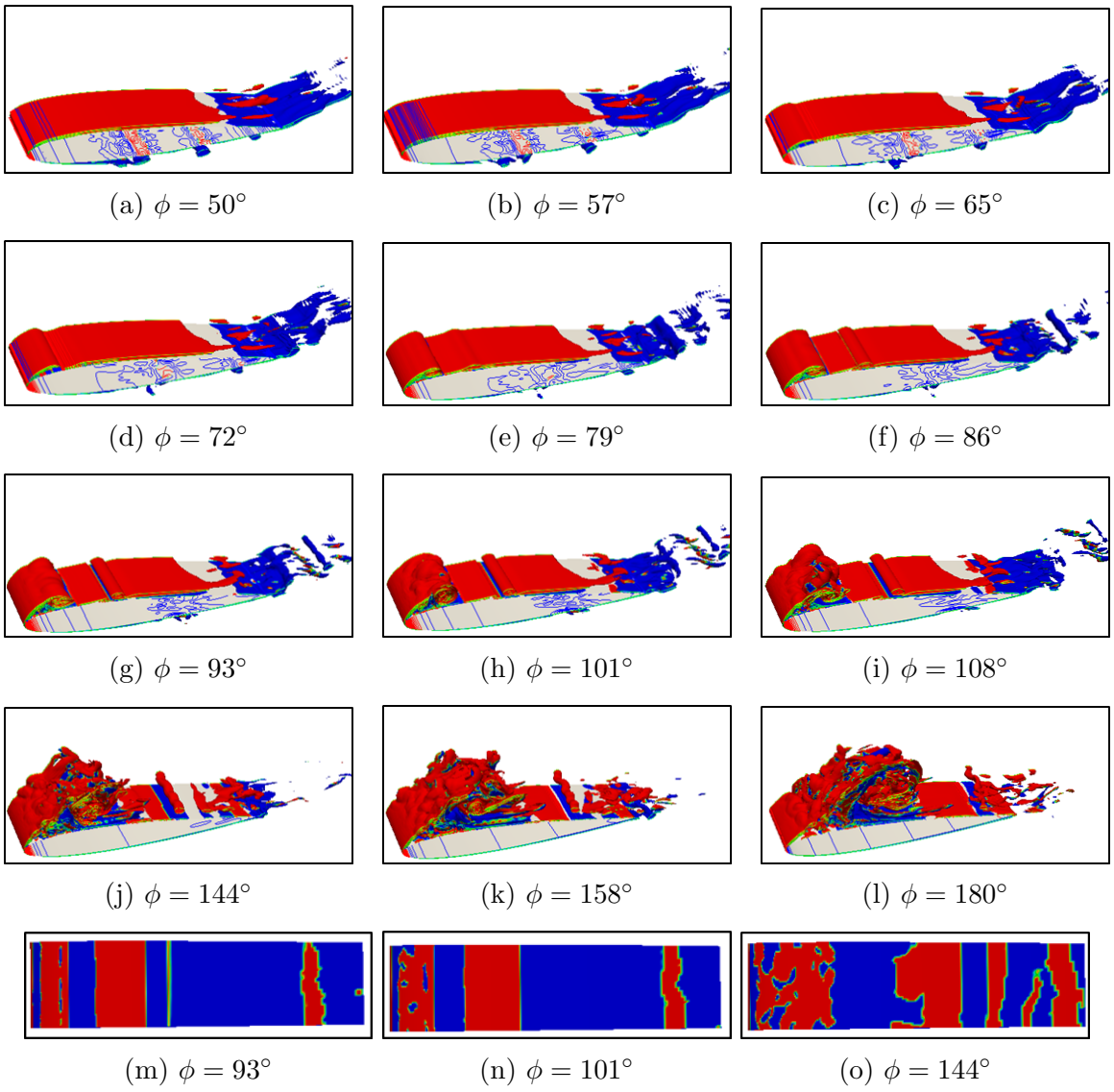

(a) $\phi = 50°$ (b) $\phi = 57°$ (c) $\phi = 65°$

(d) $\phi = 72°$ (e) $\phi = 79°$ (f) $\phi = 86°$

(g) $\phi = 93°$ (h) $\phi = 101°$ (i) $\phi = 108°$

(j) $\phi = 144°$ (k) $\phi = 158°$ (l) $\phi = 180°$

(m) $\phi = 93°$ (n) $\phi = 101°$ (o) $\phi = 144°$

Figure 8: Isosurfaces of instantaneous vorticity (a-l);instantaneous spanwise vorticity near the wing suction surface during transition (m-o) for $\alpha = 5°; k = 0.94; A/c$=0.5.

[4] Carr, L.W., McAlister, W. and McCroskey, W.J. Analysis of the development of dynamic stall based on oscillating wing experiemnt. *Tech. Rep. NASA Tech. Mem.*8382 (1977).

[5] Choi, J., Colonius, T. and Williams, D. Dynamics and energy extraction of a surging and plunging wing at low Reynolds number. *AIAA Journal.* (2013) :2013-0672.

[6] Cleaver, D.J., Gursul, I., Wang, Z. and Visbal, M.R. Lift enhancement by means of small amplitude wing oscillations at low Reynolds numbers. *AIAA Journal.* (2011) **49**:2018–2033.

[7] Ekaterinaris, J.A. and Menter, F.R. Computation of oscillating wing flows with one and two equation turbulence models. *AIAA Journal.* (1994) **32**:2359–65.

[8] Barakos, G.N. and Drikakis, D. Unsteady separated flows over maneuvering lifting surfaces. *Philos. Trans R Soc Lond.* (2000) **358**:3279–91.
[9] Wang, L., Li, L. and Fu, S. A comparative study of DES type methods for mild flow separation prediction on a NACA0015 wing. *J. Num. Mthds for Heat and Fluid Flows.* (2017) **27**:2528–2543.
[10] Visbal, M.R. High fidelity simulation of transitional flow past a plunging wing. *AIAA Journal.* (2009) **47**:2685–2697.
[11] Kim, Y. and Xie, Z.T. Modelling the effects of freestream turbulence on the dynamic stall of wind turbine blades. *J. Compt Fluids.* (2016) **129**:53–66.
[12] Jasak, H. Error analysis and estimation for the finite volume method with application to fluid flows. *PhD thesis.* Imperial College of Science, Technology and Medicine (2009).
[13] Inagaki, M., Kondoh, T. and Nagano, Y. A mixed-time-scale SGS model with fixed model-parameters for practical LES. *J. Fluids Eng.* (2005) **1**:1–13.
[14] Nicoud, F. and Ducros, F. Subgrid-scale stress modelling based on the square of the velocity gradient tensor. *J. Flow Turbul. Combust.* (1999) **62**:183–200.
[15] Chiereghin, N., Gursul, I. and Cleaver, D.J. Unsteady Measurements for a periodically plunging airfoil. *AIAA Paper.* (2017) **7**:2017-0996.
[16] Visbal, M.R. Numerical Investigation of Deep Dynamic Stall of a Plunging wing. *AIAA Journal.* (2011) **49**:2152–2170.